Diamond & Related Materials 19 (2010) 1307– 1315

Contents lists available at ScienceDirect

Diamond & Related Materials

journalhomepage:www.elsevier.com/locate/diamond

Preparation, characterization and properties of Cr-incorporated DLC fi lms on magnesium alloy

Wei Dai [a,b], Guosong Wu [a], Aiying Wang [a,□]

[a] Division of Surface Engineering, Ningbo Institute of Materials Technology and Engineering, Chinese Academy of Sciences, Ningbo 315201, China
[b] State Key Laboratory of Solid Lubrication, Lanzhou Institute of Chemical Physics, Chinese Academy of Sciences, Lanzhou 730000, China

article info

Article history:
Received 23 October 2009
Received in revised form 2 June 2010
Accepted 12 June 2010
Available online 21 June 2010

Keywords:
Magnesium alloy
Cr-DLC
Microstructure
Corrosion
Wear

abstract

Cr-incorporated diamond-like carbon (Cr-DLC) fi lms were deposited on AZ31 magnesium alloy as protective coatings by a hybrid beams deposition system, which consists of a DC magnetron sputtering of Cr target (99.99%) and a linear ion source (LIS) supplied with CH_4 precursor gas. The Cr concentration (from 2.34 to 31.5 at.%) in the fi lms was controlled by varying the fl ow ratio of Ar/CH_4. Scanning electron microscopy (SEM), transmission electron microscopy (TEM), Raman spectroscopy and X-ray photoelectron spectroscopy (XPS) were used to investigate the microstructure and composition of Cr-DLC fi lms systematically. An electrochemical system and a ball-on-disk tribotester were applied to test the corrosion and tribological properties of the fi lm on the AZ31 substrate, respectively. At low Cr doping (2.34 at.%), the fi lm mainly exhibited the feature of amorphous carbon, while at high doping (31.5 at.%), chromium carbide crystalline phase occurred in the amorphous carbon matrix of the fi lm. In this study, all the prepared Cr-DLC fi lms showed higher adhesion to AZ31 than the DLC fi lm. Especially for the fi lm with low Cr doping (2.34 at.%), it owned the lowest internal stress and the highest adhesion to substrate among all the fi lms. Furthermore, this fi lm could also improve the wear resistance of magnesium alloy effectively. But, none of the fi lms could improve the corrosion resistance of the magnesium alloy in 3.5 wt.% NaCl solution due to the existence of through-thickness defects in the fi lms.

1. Introduction

Magnesium alloys have been widely used in industry, especially in the automotive applications, due to high strength/weight ratio, excellent mechanical properties and recycle ability [1,2]. Unfortunately, it also has some disadvantages, such as the poor wear and corrosion resistance, which limit its extended utilization [3,4]. One of the effective methods to overcome the above-mentioned drawbacks is to deposit protective hard fi lms on the magnesium alloys [5]. In recent years, physical vapor deposition (PVD) technology, widely used to fabricate hard fi lms for different tribological applications, has received great attention because of environment friendliness [6]. Various kinds of fi lms, including Al, Ti, TiN and CrN produced by PVD, have been employed to improve the wear and corrosion resistances of the magnesium alloys [7– 10]. Besides above PVD fi lms, DLC fi lms were also attempted for the protection of the magnesium alloys recently due to their high hardness and wear resistance, good chemical inertness, and low friction coeffi cient [11,12]. However, a major drawback for DLC fi lms as protective coatings for magnesium alloys is their weak adhesion to the substrate because of high internal stress, which arises from the deposition mechanism known well as sub-plantation [11– 13]. Numerous metallic elements (W, Ti, Ag, Cr etc.) have been employed to modify the structures and properties of the DLC fi lms, and it was found that the metal doped into DLC fi lms (Me-DLC) played a great role in reducing internal stress and strengthening fi lm adhesion to the substrate [14– 19]. To the best of our knowledge, applying the Me-DLC fi lms on magnesium alloys as wear and corrosion protective coatings has not yet been reported till now.

Our previous work demonstrated that the Cr fi lm as a buffer-layer could signifi cantly improve the adhesion between DLC fi lm and magnesium substrate [7]. Interestingly, according to the doped metal feature in DLC fi lms mentioned in the above literatures, chromium is also one of the most effective elements in reducing stress, while not deteriorating the superior hardness, friction coeffi cient, wear and corrosion resistance of DLC fi lms [20– 22]. Thus, Cr doping seems a potential method for replacing the addition of Cr buffer-layer to improve the preparation effi ciency with reducing the process of buffer-layer preparation. Based on this consideration, a hybrid beams deposition system, including a DC magnetron sputtering of Cr target (99.99%) and a linear ion source (LIS) supplied with CH_4 precursor gas, was tried to prepare Cr-DLC fi lms on AZ31 magnesium alloy for improving the properties of AZ31 substrate. Subsequently, the microstructure, corrosion behavior and tribological properties of the Cr-DLC coated AZ31 magnesium alloy are systematically investigated.

□ Corresponding author. Tel.: +86 574 86685170; fax: +86 574 86685159.
E-mail address: aywang@nimte.ac.cn (A.Y. Wang).

0925-9635/$ – see front matter © 2010 Elsevier B.V. All rights reserved.
doi:10.1016/j.diamond.2010.06.018

2. Experiment

As-extruded AZ31 plates and silicon (100) wafers of thickness 525± 15 μm were used as the substrate materials. And a thin silicon (100) wafer of thickness 285±5 μm was also used as substrate to accurately estimate the internal stress. The AZ31 plates were first ground with emery paper up to 1500# and then polished with Al_2O_3 paste (average size 1 um). All the substrates were cleaned ultrasonically in acetone, ethanol, and dried in air before putted into the vacuum chamber. The Cr-DLC films were prepared on the AZ31 and silicon substrates by a hybrid ion beams deposition system consisting of a DC magnetron sputtering with a 120 mm (W)×380 mm (L) rectangular Cr target (99.99%) and a 380 mm (L) linear anode-layer ion sources (LIS). With this configuration of hybrid plasma sources, the ion energy of hydrocarbon ions and the doping Cr ions can be easily controlled without interruption, and the films with large uniformity area at 300 mm length (Thickness fluctuation b 5%) can be obtained, which is an ideal candidate for the industrialization. Prior to deposition, the substrates were sputter-cleaned for 20 min using Ar ion with a bias voltage of −100 V. The base pressure was evacuated to a vacuum of 2×10^{-5} Torr. During film deposition process, hydrocarbon gas (CH_4) was introduced into the linear ion source to obtain the hydrocarbon ions for DLC deposition. The Ar sputtering gas was supplied to the magnetron sputter for Cr sputtering. The concentration of chromium in the films was controlled by varying the Ar/CH_4 ratio in the supply gas mixture. The total gas flux was kept at 80 sccm and the work pressure was kept at about 3.5×10^{-3} Torr. Typical values of LIS voltage and current were 1100±20 V and 0.2 A, respectively. The DC power supplied to the sputtering gun was about 950 W (380 V, 2.5 A). A negative pulsed bias voltage of −50 V (350 KHz, 1.1 μs) was applied to the substrate. The deposition time was 1 h. For comparison, the DLC film was also prepared using LIS and a negative substrate bias of −50 V without operating the magnetron sputtering.

The thickness of the deposited films was measured by a cross-section SEM measuring scale. The chemical composition of the films was analyzed by the energy dispersive X-ray spectroscopy (EDS, Hitachi S-4800). Raman spectroscopy with an incident Ar^+ beam at a wavelength of 514.5 nm was used to measure the atomic bonds of films. High-resolution transmission electron microscopy of the films was performed on Tecnai F20 electron microscope operated at 200 keV with a point-to-point resolution of 0.24 nm. The TEM specimens were prepared by peeling off the films from the NaCl crystalline substrates, which were dissolved in deionized water. An X-ray photoelectron spectroscopy (XPS, Axis ultraDLD, Japan) with Al (mono) Kα irradiation at pass energy of 160 eV was used to characterize the chemical bonds and microstructure of the films.

The internal stress of the films was calculated from the curvature of film/substrate composite using the Stoney equation, and the curvature of film/substrate composite was determined by a laser tester. The adhesion of the films to the AZ31 substrate was assessed by a scratch tester (J&L Tech, Korea) performed on a Rockwell diamond indenter with a conical tip of 0.2 mm in radius. The critical loads at which the films failed owing to breakage were used as a criterion of the adhesive strength. In order to investigate the interface state of the film and substrate, the Cr-DLC films with the thickness of about 100 nm were deposited on the AZ31 substrates specially. XPS in-depth etching with an argon-ion gun and 3 keV ions was used to character the evolution of the composition and chemical states around interface.

For the electrochemical investigation, the experiments were performed on an AUTOLAB PGSTAT302 advanced electrochemical system, using the conventional three-electrode technique. The potential was referred to a saturated AgCl electrode (SCE) and the counter electrode was a platinum sheet. Each specimen was masked by paraffin waxes with the surface area of 1 × 1 cm^2 exposed in 3.5 wt.% NaCl solutions. These tests were carried out at 1 mV/s at room temperature. After corrosion test, the photographs of the specimen surfaces were observed using optics microscope (Leica DM2500 M, Ger). The tribological behaviors of the AZ31 coated by the films were measured on a rotary ball-on-disk tribometer at room temperature with a relative humidity of 40 ~ 50% under dry sliding conditions. A steel ball (SUJ-2, HRC60) with a diameter of 7 mm was used as the friction counter body. All the tests were performed at 0.1 m s^{-1} sliding velocity for a distance of 100 m and the applied load was 1 N. After friction test, the wear traces were measured by a surface profiler and SEM. The composition of the wear scar and debris were analyzed with EDS.

3. Results and discussion

3.1. Coating characteristic

The Cr/C atomic ratio of the as-deposited films was measured by EDS. Fig. 1 presents the Cr concentration of the films as a function of the Ar/CH_4 ratio. The average Cr concentration of the films monotonically increased from 2.34 to 31.5 at.% as the ratio of the Ar/CH_4 increased from 53/27 to 60/20. In the further text, we would use the terms "Cr-DLC-L, Cr-DLC-M and Cr-DLC-H" to denote the Cr-DLC films with 2.34 at.% (Low Cr doping), 12.1 at.% (Medium Cr doping) and 31.5 at.% (High Cr doping), respectively. Fig. 2 shows the plan-view SEM images of the films deposited on AZ31 and the cross-sectional SEM images of the films deposited on Si wafers. Obviously, the DLC film displayed a typical smooth amorphous surface morphology while partially cracked and peeled off from the AZ31 substrate due to the poor adhesion strength. However, with incorporating Cr into DLC matrix, all Cr-DLC films exhibited the good adhesion to the AZ31 substrate and no localized delamination of the films occurred. Different from the amorphous DLC morphology, all Cr-DLC films were composed of the small and compact spherical particles, and with the increase of the Ar/CH_4 ratio, the size of these particles increased and the segregated bigger "flowerlike" structure was observed. The film thickness deduced from the cross-section images increased from 641 nm for the DLC film to 780 nm for the Cr-DLC-H film, implying that the Cr doping would improve the growth rate of the films deposited by the hybrid beams.

The chemical bonds of the deposited films could be observed from the XPS spectra. Fig. 3 shows the XPS C 1s peaks of the pure DLC and Cr-DLC films. The C 1s spectra of the DLC film only revealed a single peak around 284.6 eV corresponding to the typical C–C or C–H binding energy of the DLC film [23]. With the incorporation of Cr atoms, a shoulder peak with a lower binding energy of 283 eV appeared, and the peak intensity increased with the Cr concentration increasing. Since the peak at 283 eV is generally assigned to the Cr–C bonds [19], it can be deduced that the chromium carbide was formed in the films and the fraction of the carbide increased as the Cr concentration increased.

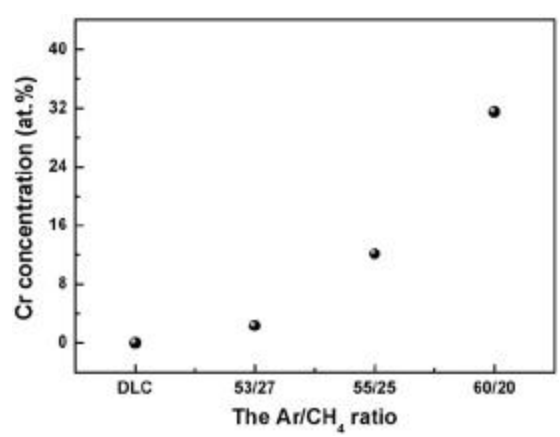

Fig. 1. Cr concentration of the deposited films as a function of the Ar/CH_4 ratio.

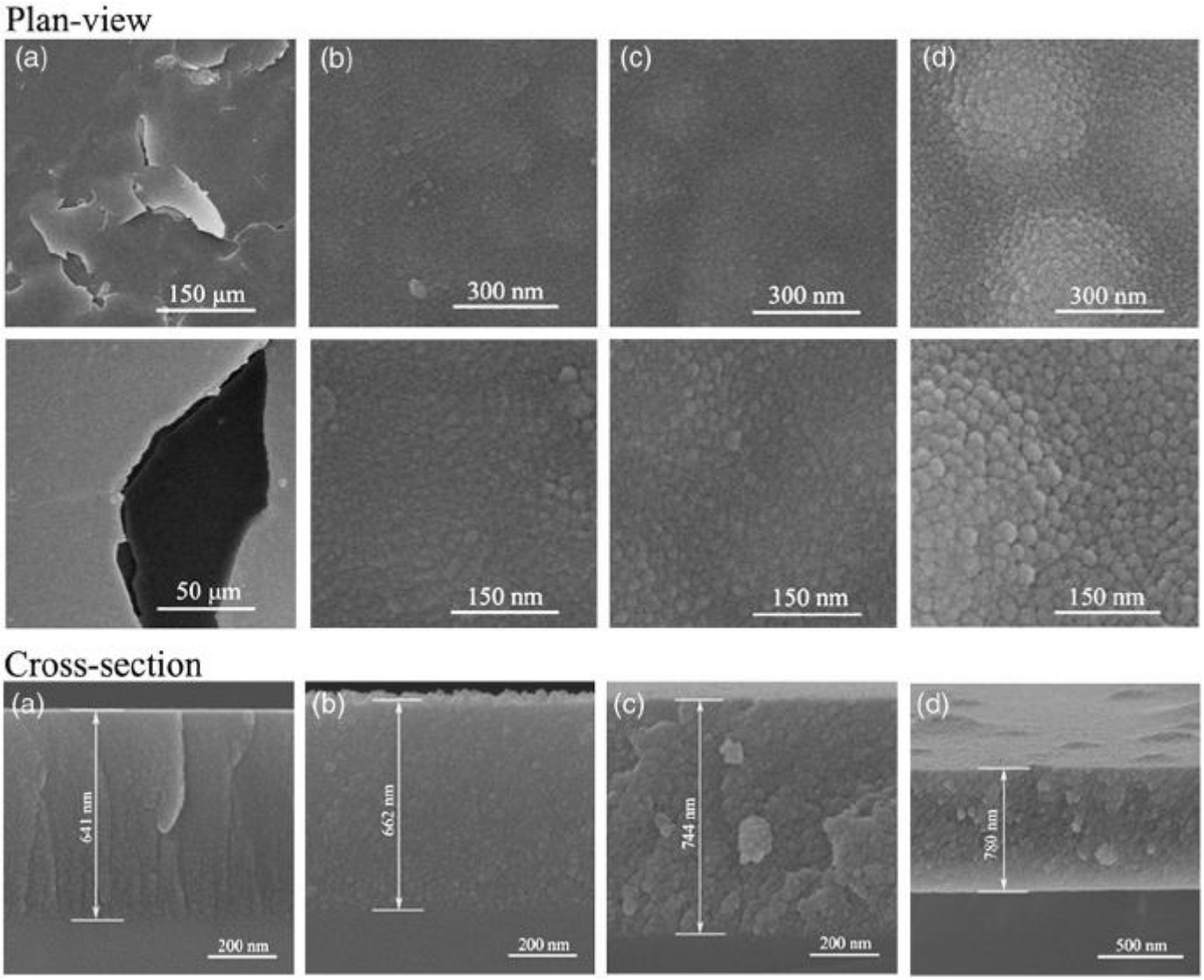

Fig. 2. Plan-view SEM images of the films deposited on AZ31 and cross-sectional SEM images of the films deposited on Si wafers: (a) DLC, (b) Cr-DLC-L, (c) Cr-DLC-M, and (d) Cr-DLC-H.

Fig. 4 shows the plan-view TEM images and corresponding sectional area electron diffraction (SAED) patterns of the DLC film and Cr-DLC films. The pattern of the DLC film (Fig. 4(a)) presented a diffuse halo, representing the typical amorphous structure. For Cr-DLC-L (Cr 2.34 at.%), although the XPS result of Fig. 3 revealed that a small amount of Cr– C bonds were formed in this film, the SAED pattern was similar to that of the pure DLC and showed a ringlike pattern, which indicated that crystal phases began to evolve in the amorphous carbon matrix of the film. For Cr-DLC-H (Cr 31.5 at.%), sharp crystalline diffraction rings were clearly observed in Fig. 4(c). Those rings could be identified to be the (111), (200), (220) and (311) reflections of the face-centered (FCC) chromium carbide structure with a lattice parameter of 0.413 nm. This lattice parameter was very close to the lattice parameter of B1 CrC (0.41 nm), which implying that the CrC crystalline phase was formed in the carbon films at high doping.

The representative Raman spectra of the DLC and Cr-DLC films are shown in Fig. 5(a). There is a broad asymmetric Raman scattering band in the range of 1000– 1700 cm^{-1}, representing the typical characteristic of DLC film [12]. It is found that the intensity of the Raman spectra decreased as the ratio of Ar/CH_4 increased. The phenomenon perhaps attributed to that, the Cr incorporation resulted in the decrease of the carbon fraction in per unit area of the film, which would reduce the Raman scattering cross-section of the film, and thus caused the film scattering intensity decrease.

Usually, the Raman spectra of DLC films can be fitted using two Gaussians peaks, the G peak and the D peak, as shown in the insert figure of Fig. 5(a). The G peak centered at around 1550 cm^{-1} is due to the bond stretching of all pairs of sp^2 atoms in both aromatic rings and carbon chains, and the D peak is due to the breathing modes of sp^2 atoms only in rings. According to the G peak position and the intensity ratio of D peak to G peak (I_D/I_G), the sp^2/sp^3 ratio of the DLC films can be characterized [24]. As the sp^2/sp^3 ratio decreases in hydrogenated amorphous carbon, the G peak and the I_D/I_G ratio will move down and decrease, respectively [12,24]. The corresponding G peak position and the I_D/I_G ratio of the films, after fitted, are clarified in Fig. 5(b). The G peak position shifted towards high wave number and the I_D/I_G ratio also increased in the Cr-DLC films, implying the higher sp^2/sp^3 ratio in the Cr-DLC films as compared with that in the DLC films. When the Ar/CH_4 ratio increased further, the sp^2/sp^3 ratio decreased subsequently according to the downshift of the G peak and the decrease of the I_D/I_G ratio. The initial increase of the sp^2/sp^3 ratio due to Cr doping might attribute to the catalyst effect of Cr atoms on the formation of sp^2 sites [25,26]. However, since sp^2-C has the relative lower bonding energy than sp^3-C, it would favor to bonded with the Cr atoms to form the CrC phase. Consequently, as Cr concentration increased, a larger number

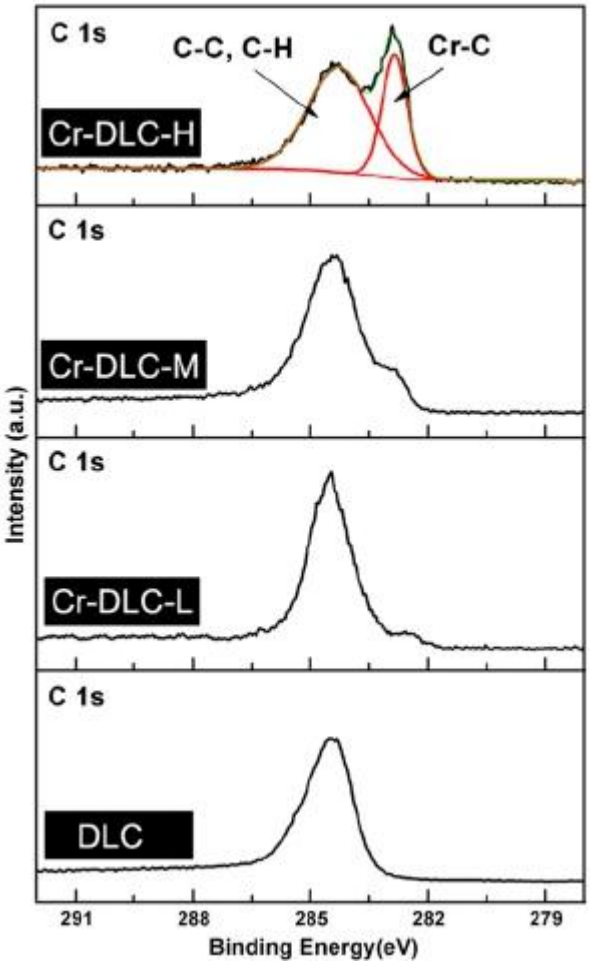

Fig. 3. Typical C 1s high-resolution XPS spectra of DLC film and Cr-DLC films.

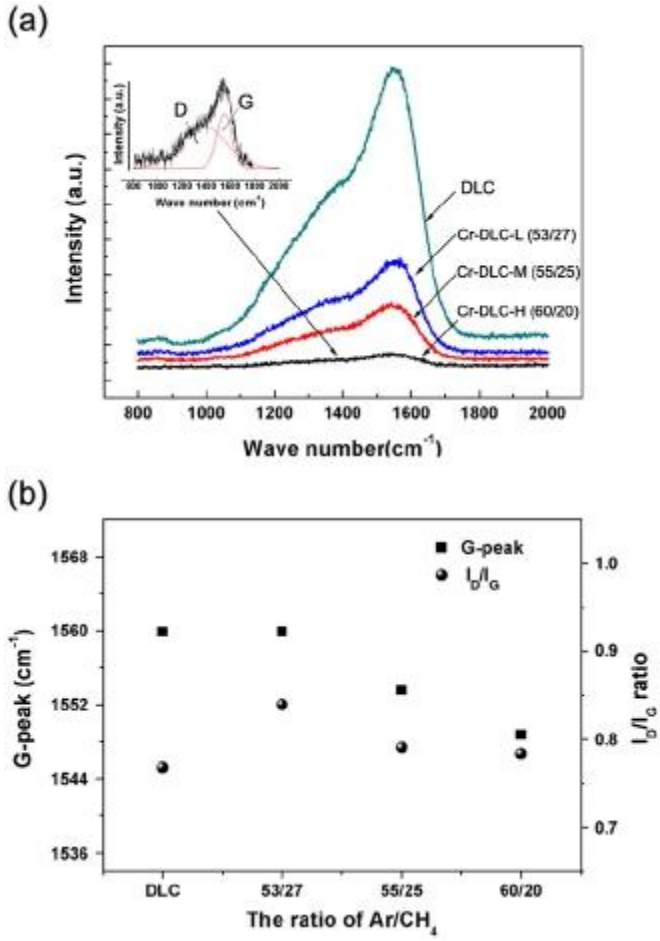

Fig. 5. (a) Representative Raman spectra and (b) corresponding G peak position and I_D/I_G of the films.

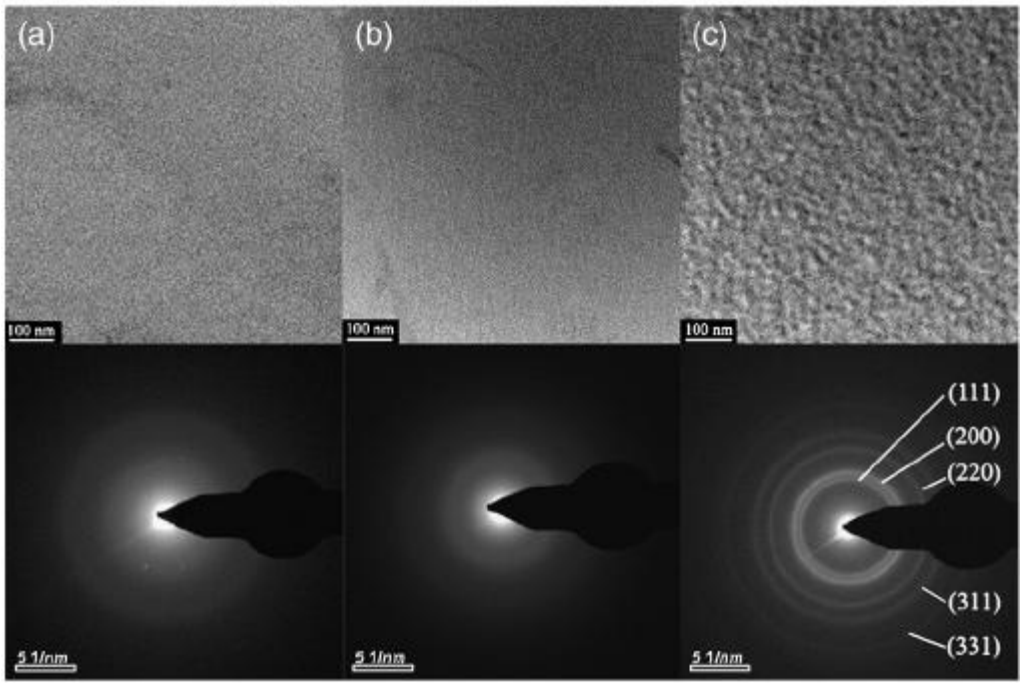

Fig. 4. Typical TEM micrograph and corresponding diffraction pattern of (a) DLC, (b) Cr-DLC-L, and (c) Cr-DLC-H.

of sp^2-C were used to formed carbide phase and thus resulted in the decrease of sp^2-C fraction. Similar influence of the metal doping on the sp^2/sp^3 ratio was also observed in Mo-DLC, where Mo bonded with sp^2-C and thus caused the sp^2/sp^3 ratio decrease [27].

Fig. 6 shows the internal stress of the DLC film and Cr-DLC films deposited at different Ar/CH_4 ratios. The internal stress dramatically decreased at first and then increased as the Ar/CH_4 ratio increased further, and the lowest internal stress was acquired by the Cr-DLC-L film. The most important factor of the internal stress reduction was the increase of the sp^2 fraction in the Cr-DLC film due to Cr doping (see Fig. 5), since the sp^2 bond has been expected to relieve the compressive stress [12,28]. In addition, Wang et al. [29] also proposed that the metal atoms distributed in the amorphous carbon matrix play a role of a pivotal site, whereby distortion of the atomic bond angles can occur without inducing a significant increase in the elastic energy. The internal stress can be relaxed through the atomic bond distortion. At high Cr doping, however, many CrC phases were formed in the amorphous carbon matrix. Since the Cr– C bond length is longer than the C– C bond length, it would cause the internal stress increase.

To obtain the high adhesion is one of the major technology challenges for the DLC protective films on magnesium alloy, and it has vital influences on the wear and corrosion resistance of the films. Fig. 7 shows the critical loads of the DLC and Cr-DLC films coating on AZ31. The results showed that in general, all Cr-DLC films revealed much higher critical load than the DLC film, and the Cr-DLC-L film with the lowest internal stress exhibited the highest critical load. Normally, the internal stress has significant influence on the adhesive strength of DLC films. However, the Cr-DLC-M and Cr-DLC-H films still showed higher adhesion than the DLC film, although they possessed relatively high internal stress. Obviously, the addition of Cr atoms was helpful to the improvement of the film adhesion. This indicates that the achievement of the good interface adhesion was not only due to the low internal stress but also due to the strong interface bonding.

3.2. Interface analysis of Cr-DLC/AZ31

The chemical state of the interface between the film and the AZ31 substrate was performed by XPS in-depth etching using an argon-ion gun with 3 KeV ions. Fig. 8 presents the C 1s, Cr 2p, Mg 2p and O 1s high-resolution XPS spectra of the AZ31 coated by Cr-DLC films with a thickness of about 100 nm against etching depth as well as etching time. Each etching time corresponds to a certain depth (between the film and substrate). As the etching depth increased, the intensities of the C 1s and Cr 2p spectra decreased, while the relative intensity of the Mg 2p spectra increased. The C 1s XPS spectra could be also deconvoluted into two main peaks, similar to those in Fig. 3. However, the relative intensity of Cr– C peak in the C 1s spectra of Fig. 8(a) seemed to be higher than that in Fig. 3 (Cr-DLC-L), implying higher

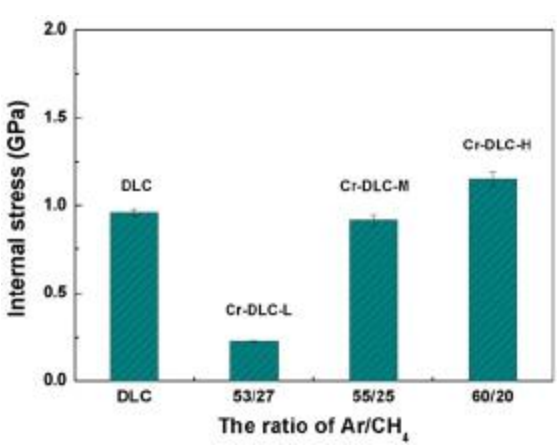

Fig. 6. Internal stress of DLC film and Cr-DLC films deposited at different Ar/CH_4 ratios.

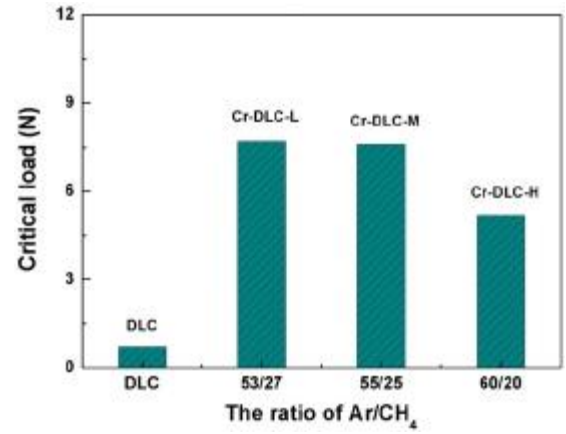

Fig. 7. Critical load of DLC film and Cr-DLC films deposited at different Ar/CH_4 ratios coating on AZ31.

concentration of Cr around the interface. The difference of Cr concentration might attribute to the "target poisoning" due to the interaction of the target with the reactive gases, which was encountered usually in Me-DLC deposition [30– 32]. At the beginning, the metal target was clear. The metal could be easily sputtered from the target. Then, the target was gradually covered by carbonaceous species, and the sputtering yield decreased until dynamical equilibrium between target covering by carbon and cleaning by argon. Accordingly, the Cr concentration in the interface (in initial step) would be higher than that in the film bulk.

For both the Cr-DLC-L and Cr-DLC-H samples, as the depth increased from depth 1 to depth 5 (from the film to AZ31), the position of the Mg 2p main peak changed from about 51.3 eV to about 50 eV. The Mg 2p peak could be deconvoluted into three composite peaks. The broad peaks at binding energies of about 51.3 eV and 50.5 eV were corresponding to Mg in magnesium carbonate state and magnesium oxide state, respectively. The single and spiked peak at about 50 eV corresponds to magnesium in the metallic state. The O 1s peak increased initially and then decreased as the etching depth increased, and it could deconvoluted into two components with binding energies of 531 eV and 534 eV corresponding to oxide and carbonate, which were consisted with the Mg 2p spectra. This clearly illustrated that the oxide layer (MgO) was still remained on the AZ31 surface. It is suggested that the interface of the films and AZ31 seems to be relatively complex, which was also reported in other literature [33].

The weak adhesive strength of the DLC film on AZ31 mainly attribute to two factors: one is the high internal stress of the DLC films, and the other is the low interfacial bonding energy due to the abrupt difference between DLC and magnesium in materials properties, such as hardness, elastic modulus, and melting points [34]. The improvement of the adhesion between the Cr-DLC films and AZ31 might be accounted for the existence of chromium in the interface. Thus, the film/AZ31 interface was able to endure the high internal stress in the Cr-DLC-H film.

3.3. Corrosion behavior

The polarization curves of all specimens are shown in Fig. 9. By using the Tafel region extrapolation from the polarization curves, the corrosion current density and potential were obtained and illustrated in Table 1. All the AZ31 coated by the Cr-DLC films exhibited higher corrosion potential than the bare AZ31. However, all the as-deposited films didn't reduce the corrosion current density of the coated AZ31 compared with that of the bare AZ31. This indicated that neither the DLC film nor the Cr-DLC films could improve the corrosion resistance

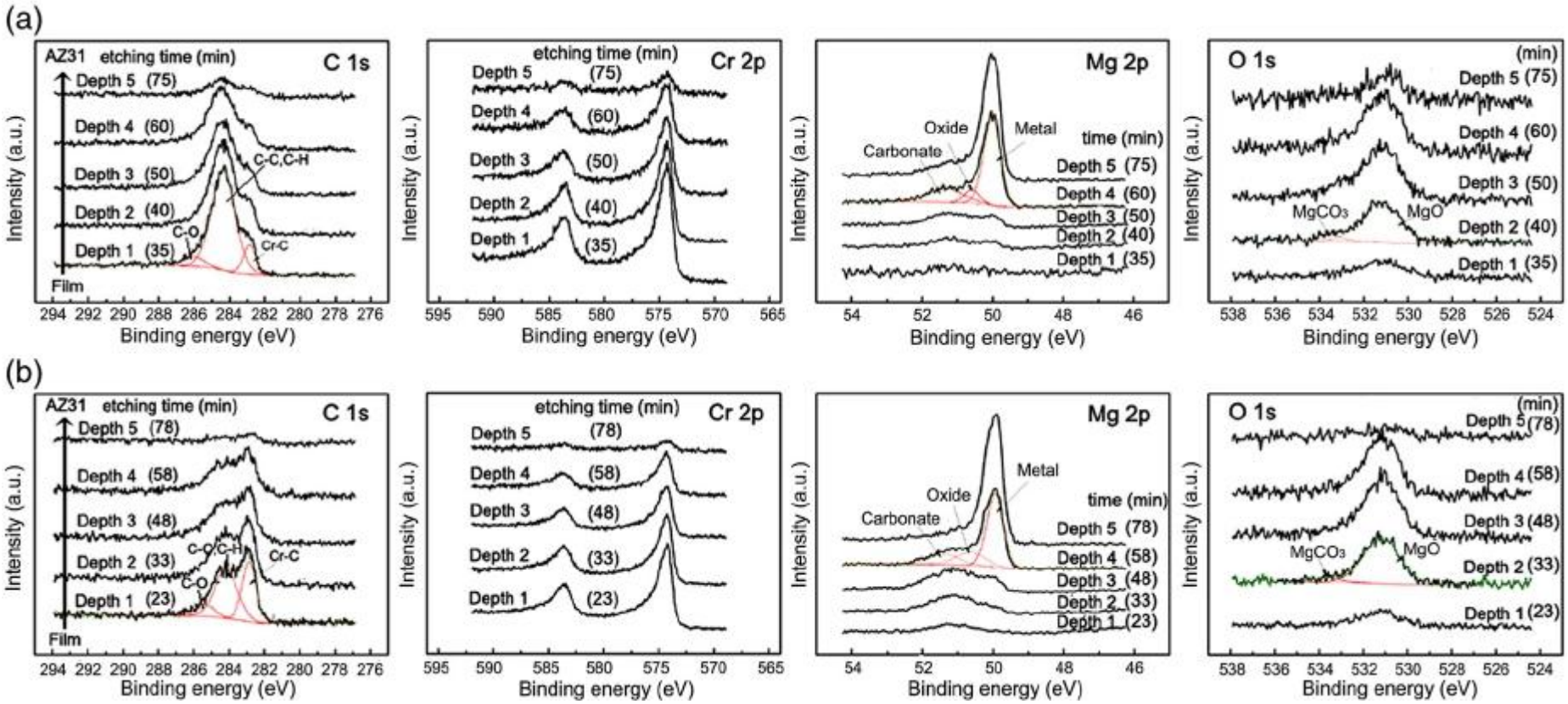

Fig. 8. Typical high-resolution C 1s, Cr 2p, Mg 2p and O 1s spectra of (a) Cr-DLC-L and (b) Cr-DLC-H coating on AZ31 against etching depth as well as etching time in the in-depth XPS analysis.

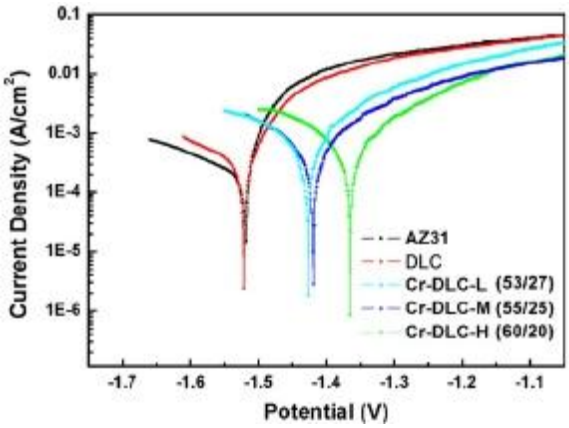

Fig. 9. Polarization curves of DLC film and Cr-DLC films coating on AZ31.

Table 1
Electrochemical parameters obtained from the polarization curves of Fig. 9.

Sample	Corrosion potential (V)	Corrosion current density (A/cm2)
AZ31	− 1.519	1.863 × 10− 4
DLC	− 1.521	3.023 × 10− 4
Cr-DLC-L	− 1.427	5.896 × 10− 4
Cr-DLC-M	− 1.420	5.465 × 10− 4
Cr-DLC-H	− 1.367	6.543 × 10− 4

of the magnesium alloy, since the corrosion current was directly related to the corrosion rate.

Fig. 10 shows the photographs of the specimen surfaces after corrosion test. It is observed that the DLC film in the DLC/AZ31 specimen was completely broken and destroyed in corrosion due to the poor adhesion. For the Cr-DLC/AZ31 specimens, some large corrosion pits were observed on the surface. Altun et al. proposed that the through-thickness defects, like micro-pits and -pores in the coating, are the main factor to influence the corrosion resistance of the AlN PVD coating/magnesium substrate system [35,36]. Although the growth mode of the amorphous DLC film is different from that of the columnar AlN film, there are still some pores, even in good quality PVD or CVD DLC films [37,38]. Corrosive solution can penetrate the DLC coating via those through-thickness pores and attack the AZ31 substrate to form local galvanic corrosion. With the gradually evolution of the local corrosion, corrosion pits were gradually enlarged and at last presented the morphology as shown in Fig. 10.

3.4. Tribological properties

Fig. 11(a) presents the coefficient of friction (COF (μ)) of the AZ31 coated by the films against sliding distance. The bare AZ31 was also performed in tribological experiment for comparison. The Cr-DLC-L and Cr-DLC-M specimens showed a relative stable friction-distance profile, and the average friction coefficient was about 0.3 lower than 0.4 for the bare AZ31. However, even the DLC and Cr-DLC-H specimens also exhibited low friction coefficient about 0.3 in initial step, the non-stable friction behavior with continuous oscillatory peaks was viewed after a few meters sliding (about 3 m and 6 m for DLC and Cr-DLC-H, respectively), which was similar to the results tested for the bare AZ31 alloy. Fig. 11(b) shows the surface profiles of the wear tracks in the uncoated and coated AZ31. The DLC and Cr-DLC-H specimens presented deep and broad wear tracks, as the uncoated AZ31 showed. On the contrary, the wear track of the Cr-DLC-L specimen was smooth and unnoticeable.

To investigate the wear mechanism of the Cr-DLC films on AZ31 substrate, the SEM morphology was used to obtain the wear scar and debris composition of the films after friction tests. Fig. 12 shows the details morphologies with the inserted magnified images and the

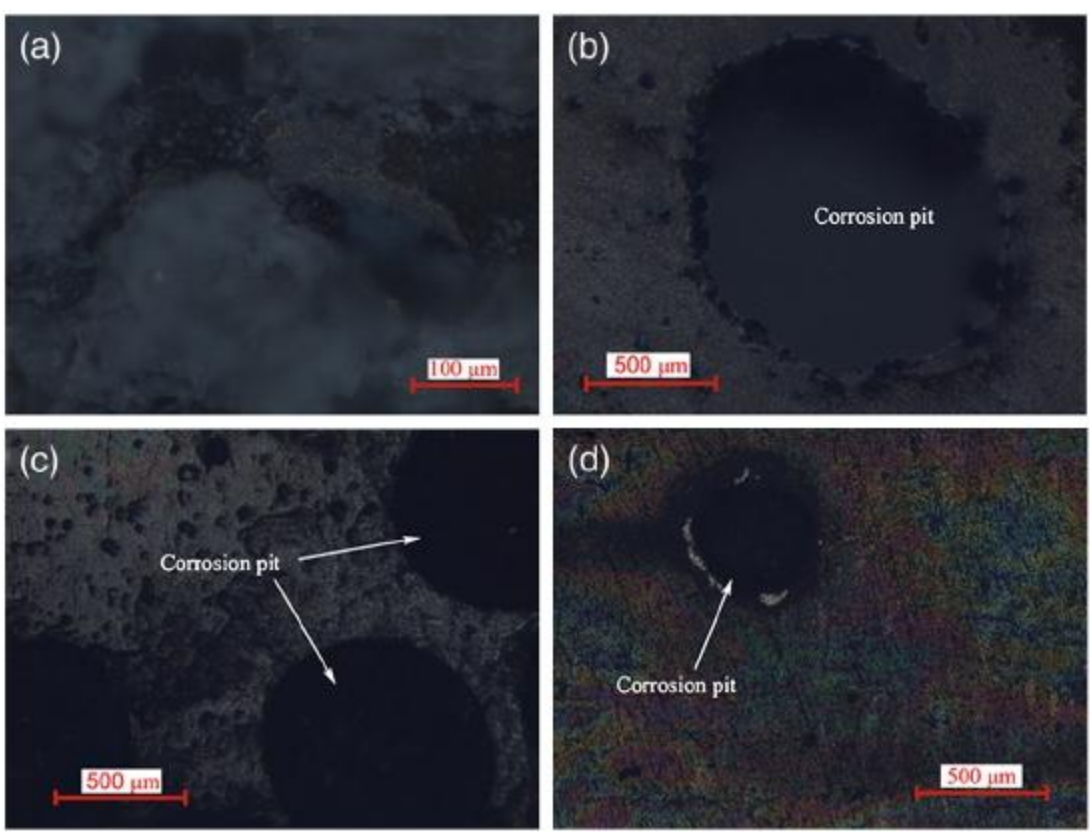

Fig. 10. Surface micrograph of the AZ31 substrate coated by (a) DLC, (b) Cr-DLC-L, (c) Cr-DLC-M, and (d) Cr-DLC-H after corrosion test.

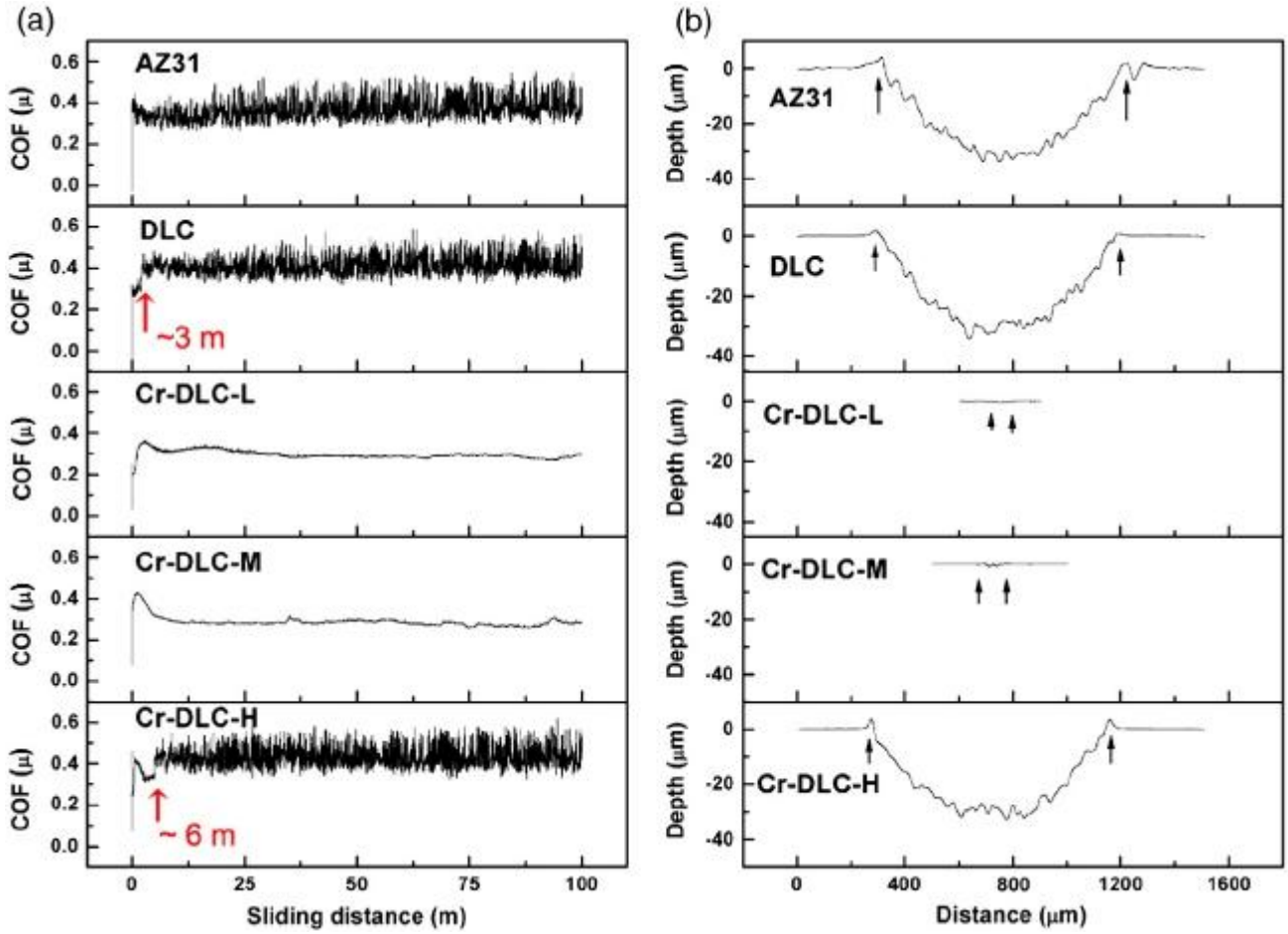

Fig. 11. (a) Coefficient of friction (COF) of bare AZ31 and the films coating AZ31 as a function of sliding distance, and (b) corresponding surface profiles of the wear tracks after friction test.

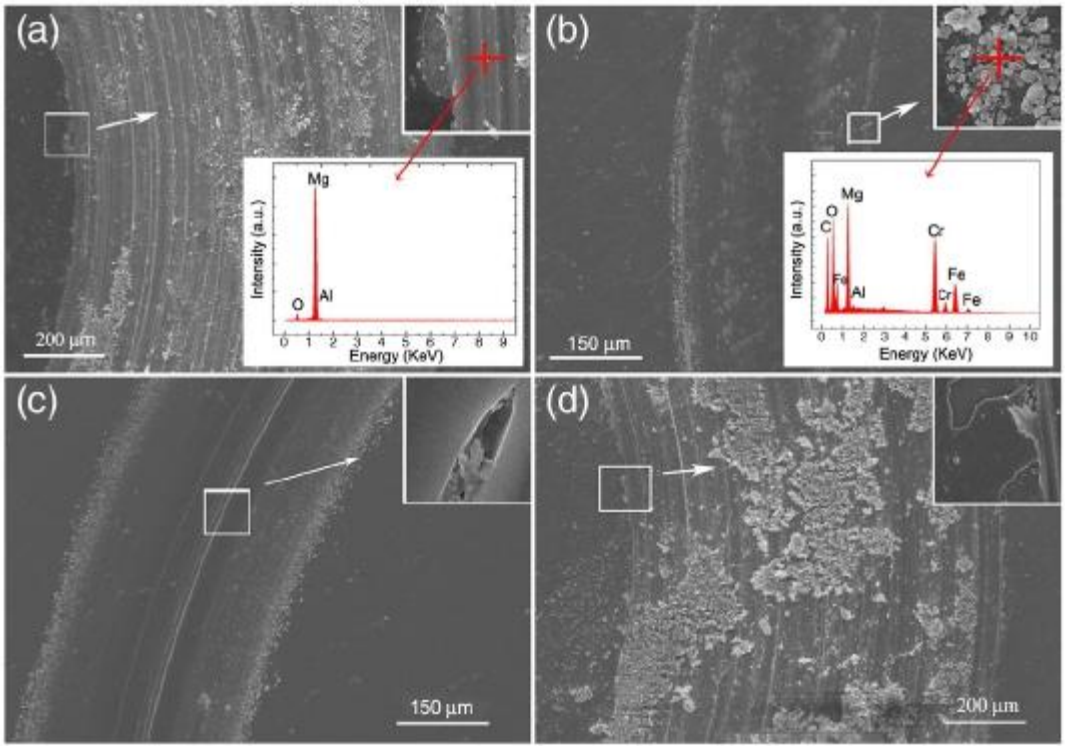

Fig. 12. SEM images and EDS analysis of the wear tracks on (a) DLC, (b) Cr-DLC-L, (c) Cr-DLC-M, and (d) Cr-DLC-H.

partially elaborated chemical composition by EDS. It is observed that the DLC and Cr-DLC-H films were completely peeling off from AZ31 substrate in wear process, as shown in the insert of Fig. 12(a) and (d), and it is confirmed that no carbon element was detected from the wear trace by the EDS analysis. As a consequence, the sudden increase of the friction coefficient on the DLC and the Cr-DLC-H film mainly attributed to the films failure. The Cr-DLC-L specimen exhibited excellent wear resistance and the durable wear life during the friction. Noted that numerous small pieces of wear debris were accumulated along the wear track, and a large amount of C, O, Fe was observed from the EDS analysis, as shown in the insert of Fig. 12(b). This reveals that, during the friction, the formation of oxide due to the temperature spikes occurred at asperity contacts between the counter-body steel ball and the film [19]. In other aspect, the detected C element denotes that the Cr-DLC film was survived during all the sliding. Fig. 12(c) and the inset showed that the Cr-DLC-M specimen processed more serious wear than the Cr-DLC-L due to that more wear debris and cracks were observed in the wear track. In conclusion, the Cr-DLC-L film could greatly improve the wear resistance of the AZ31 magnesium alloy in this study.

4. Conclusions

The Cr-DLC films with various Cr concentrations were successfully deposited on AZ31 by the hybrid beams system, including a linear ion source and a magnetron sputtering source. The concentration of chromium in the films was varied from 2.34 at.% to 31.5 at.% by changing the Ar/CH_4 ratio in the gas mixtures with a total flow rate at 80 sccm. At low Cr doping (2.34 at.%), the film mainly exhibited the feature of amorphous carbon, whereas at high doping (31.5 at.%), chromium carbide crystalline phase occurred in the amorphous carbon matrix of the film. All the Cr-DLC films showed higher adhesion to AZ31 substrate compared with that of the DLC film. None of them could distinctly improve the corrosion resistance of the magnesium alloy systems in 3.5 wt.% NaCl solution due to the formation of galvanic cell in through-thickness defects of the films. However, the Cr-DLC film with low Cr concentration (2.34 at.%) exhibited a relatively low friction coefficient and a good wear resistance in this study. It is noticeable that, we showed a possibility to fabricate the DLC protective coatings with high adhesion strength and good wear resistance for the magnesium alloy without any addition of interlayer.

Acknowledgements

The project was supported by Zhejiang Province Key Technologies R & D Program (Grant No. 2008C21055, 2009C11SA550048). One of the authors, Guosong Wu, thanks the financial support from China Postdoctoral Science Foundation (Grant No. 20080430694) and Shanghai Postdoctoral Scientific Program (Grant No. 08R214156).

References

[1] R. Ambat, N.N. Aung, W. Zhou, Corros. Sci. 42 (2000) 1433.
[2] Y. Kojima, Mater. Sci. Forum 350– 351 (2000) 3.
[3] J. Dutta Majumdar, R. Galun, B.L. Mordlike, I. Manna, Mater. Sci. Eng. A 361 (2003) 119.
[4] H. Hoche, H. Scheerer, D. Probst, E. Broszeit, C. Berger, Surf. Coat. Technol. 174– 175 (2003) 1002.
[5] J.E. Gray, B. Luan, J. Alloys Compd. 336 (2002) 88.
[6] H. Hoche, H. Scheerer, D. Probst, E. Broszeit, C. Berger, Surf. Coat. Technol. 174– 175 (2003) 1018.
[7] G.S. Wu, L.L. Sun, W. Dai, L.X. Song, A.Y. Wang, Surf. Coat. Technol. 204 (2010) 2193.
[8] G.S. Wu, K.J. Ding, X.Q. Zeng, X.M. Wang, S.S. Yao, Scr. Mater. 61 (2009) 269.
[9] H. Altun, H. Sinici, Mate. Charact. 59 (2008) 266.
[10] Y. Shi, S. Long, L. Fang, F. Pan, H. Liao, Appl. Surf. Sci. 255 (2009) 6515.
[11] N. Yamauchi, N. Ueda, A. Okamoto, T. Sone, M. Tsujikawa, S. Oki, Surf. Coat. Technol. 201 (2007) 4913.
[12] J. Robertson, Mater. Sci. Eng., R 37 (2002) 129.
[13] A.C. Ferrari, S.E. Rodil, J. Robertson, W.I. Milne, Diamond Relat. Mater. 11 (2002) 994.
[14] Y. Pauleau, E. Thiery, Surf. Coat. Technol. 180 (2004) 313.
[15] K.I. Schiffmann, Surf. Coat. Technol. 177 (2004) 453.
[16] A.Y. Wang, H.S. Ahn, K.R. Lee, J.P. Ahn, Appl. Phys. Lett. 86 (2005) 111902.
[17] S. Zhang, X.L. Bui, J. Jiang, X. Li, Surf. Coat. Technol. 498 (2005) 206.
[18] R.J. Narayan, Diamond Relat. Mater. 14 (2005) 1319.
[19] V. Singh, J.C. Jiang, E.I. Meletis, Thin Solid Films 189 (2005) 150.
[20] C. Donnet, Surf. Coat. Technol. 100– 101 (1998) 180.
[21] D.Y. Wang, Y.Y. Chang, C.L. Chang, Y.W. Huang, Surf. Coat. Technol. 200 (2005) 2175.
[22] Y.Y. Chang, D.Y. Wang, W. Wu, Thin Solid Films 420– 421 (2002) 241.
[23] D. Bourgoin, S. Turgeon, G.G. Ross, Thin Solid Films 357 (1999) 246.
[24] C. Casiraghi, A.C. Ferrari, J. Robertson, Phys. Review. B 72 (2005) 085401.
[25] Y.Y. Chang, D.Y. Wang, W.T. Wu, Thin Solid Films 420– 421 (2002) 241.
[26] C. Corbella, E. Bertran, M.C. Polo, E. Pascual, Diamond Relat. Mater. 16 (2007) 1828.
[27] L. Ji, H. Li, F. Zhao, J. Chen, H. Zhou, Diamond Relat. Mater. 17 (2008) 1949.
[28] B.K. Tay, Y.H. Cheng, X.Z. Ding, S.P. Lau, X. Shi, G.F. You, D. Sheeja, Diamond Relat. Mater. 10 (2001) 1082.
[29] A.Y. Wang, K.R. Lee, J.P. Ahn, J.H. Han, Carbon 44 (2006) 1826.
[30] O.A. Fouad, Abdul K. Rumaiz, S. Ismat Shah, Thin Solid Films 517 (2009) 5689.
[31] I. Safi, Surf. Coat. Technol. 127 (2000) 203.
[32] G. Zhang, P. Yan, L. Wang, P. Wang, Y. Chen, J. Zhang, J. Phys. D Appl. Phys. 40 (2007) 6748.
[33] G.S. Wu, X.Q. Zeng, G.Y. Yuan, Mater. Lett. 62 (2008) 4325.
[34] Thaddeus B. Massalski (Ed.), Binary Alloy Phase Diagrams, vol. 2, American Society of Metals, Metal Park, Ohio 44073, 1986, p. 1544.
[35] H. Altun, S. Sen, Mater. Des. 27 (2006) 1174.
[36] H. Altun, S. Sen, Surf. Coat. Technol. 197 (2005) 193.
[37] V. Novotny, N. Staud, J. Electrochem. Soc. Electrochem. Sci. Technol. 135 (1988) 2931.
[38] A. Zeng, E. Liu, I.F. Annergren, S.N. Tan, S. Zhang, P. Hing, J. Gao, Diamond Relat. Mater. 11 (2002) 160.